Check for updates

Earth's Future

RESEARCH ARTICLE
10.1029/2022EF003330

What Does Global Land Climate Look Like at 2°C Warming?

Taejin Park[1,2], Hirofumi Hashimoto[1,3], Weile Wang[1], Bridget Thrasher[4], Andrew R. Michaelis[1], Tsengdar Lee[5], Ian G. Brosnan[1], and Ramakrishna R. Nemani[1,2]

[1]NASA Ames Research Center, Moffett Field, CA, USA, [2]Bay Area Environmental Research Institute, Moffett Field, CA, USA, [3]California State University Monterey Bay, Monterey County, CA, USA, [4]Climate Analytics Group, Menlo Park, CO, USA, [5]NASA Headquarters, Washington, DC, USA

Key Points:

- CMIP6 models show that the Earth likely will reach 2°C of global warming by the 2040s without significant policy changes
- Geographic pattern of changes in key climate indicators portend unfavorable conditions of habitability for large populations
- Downscaled climate projections provide finer scale spatial patterns that enable region-specific climate adaptation and mitigation strategies

Supporting Information:

Supporting Information may be found in the online version of this article.

Correspondence to:

T. Park,
taejin.park@nasa.gov

Citation:

Park, T., Hashimoto, H., Wang, W., Thrasher, B., Michaelis, A. R., Lee, T., et al. (2023). What does global land climate look like at 2°C warming? *Earth's Future*, *11*, e2022EF003330. https://doi.org/10.1029/2022EF003330

Received 2 JUL 2022
Accepted 3 DEC 2022

Author Contributions:

Conceptualization: Taejin Park, Weile Wang, Ramakrishna R. Nemani
Data curation: Taejin Park, Hirofumi Hashimoto, Bridget Thrasher, Andrew R. Michaelis
Formal analysis: Taejin Park
Funding acquisition: Tsengdar Lee, Ian G. Brosnan, Ramakrishna R. Nemani
Investigation: Taejin Park
Methodology: Taejin Park
Project Administration: Ian G. Brosnan, Ramakrishna R. Nemani
Software: Taejin Park

© 2022 The Authors. Earth's Future published by Wiley Periodicals LLC on behalf of American Geophysical Union. This is an open access article under the terms of the Creative Commons Attribution License, which permits use, distribution and reproduction in any medium, provided the original work is properly cited.

Abstract Constraining an increase in global mean temperature below 2°C compared to pre-industrial levels is critical to limiting dangerous and cascading impacts of anthropogenic climate change. Understanding future climatic changes and their spatial heterogeneity at 2°C warming is thus important for policy makers to prepare actionable adaptation and mitigation plans by identifying where and to what extent lives and livelihoods will be impacted. This study uses the recently released NASA Earth eXchange Global Daily Downscaled Projections (NEX-GDDP) CMIP6 data to provide a broad overview of projected changes in six key climate variables and two climate impact indicators at a time when warming exceeds 2°C. Analysis of global mean temperature changes indicates the 2040s as the decade when most CMIP6 models reach 2°C warming with respect to a pre-industrial period (1850–1900). During the 2040s, we find that global mean temperature, precipitation, relative humidity, downwelling shortwave and longwave radiation, and wind speed over land under the high emission scenario are projected to change by +2.8°C, +22.4 mm/year, −0.73%, −2.23 , +15.9 W/m^2, and −0.04 m/s, respectively. Many of the future changes are expected to exacerbate climate impacts including heat stress and fire danger. Our analysis shows geographic patterns of policy-relevant climatic changes, as parts of the globe will experience significant climate impacts even if the goal to keep warming below 2°C goal is achieved. Our results highlight the urgent need for further studies focused on identifying key hotspots and advancing region-specific actionable adaptation and mitigation plans.

Plain Language Summary Robust understanding of the spatial patterns of climatic change as the world approaches 2°C warming is a priority for policy makers preparing actionable adaptation and mitigation plans. The recently released NASA Earth eXchange Global Daily Downscaled Projections (NEX-GDDP) data is a unique tool for assessing these changes with unbiased projections at 16-64 times finer spatial scale than the ones originally available. Our work uses the NEX-GDDP data to answer a simple but important question, "What does global land climate look like at 2°C warming?" We find that the Earth will likely reach 2°C of global warming by the 2040s. In the 2040s, our analysis shows significant changes in six key climate variables (mean air temperature, precipitation, relative humidity, downwelling shortwave and longwave radiation, and wind speed) but with geographically varying magnitude and direction of changes. These changes collectively result in increasing risks of heat stress and fire which already manifest as life-threatening impacts resulting from climate change. Many of the projected changes are expected to exacerbate climate impacts, and our fine scale spatial analysis reveals that parts of the globe (e.g., countries in lower latitude) will experience significant climate impacts even if pledges to limit warming to less than 2°C are achieved. This study provides a comprehensive assessment of projected climate changes under 2°C warming and highlights the urgent need for further studies focused on identifying key hotspots and advancing region-specific actionable adaptation and mitigation plans.

1. Introduction

The Earth's climate has changed rapidly since the start of the Industrial Revolution, and the role of human influence on the climate is indisputable (Masson-Delmotte et al., 2018). Human-induced global warming has already caused observed changes in the climate system. Its consequential impacts on organisms and ecosystems, as well as on human systems and well-being, are also evident (Barnett et al., 2005; Dunne et al., 2013; Fauchald et al., 2017; Hsu et al., 2021; Park et al., 2019). In response to the observed impacts and risks from climate change, the Paris Climate Agreement set a collective goal "*to hold warming well below 2°C, with efforts to limit warming to 1.5°C*" above pre-industrial averages (UNFCCC, 2015). The 2°C of warming is considered a critical

Supervision: Ian G. Brosnan, Ramakrishna R. Nemani
Visualization: Taejin Park
Writing – original draft: Taejin Park
Writing – review & editing: Taejin Park, Hirofumi Hashimoto, Weile Wang, Bridget Thrasher, Andrew R. Michaelis, Tsengdar Lee, Ian G. Brosnan, Ramakrishna R. Nemani

threshold to limit the dangerous and cascading effects of anthropogenic climate change (Masson-Delmotte et al., 2018, 2021; Schleussner et al., 2016). Therefore, robust projections and comprehensive understanding of future climate changes are important to providing reliable information with respect to climate mitigation and adaptation.

General circulation models (GCMs) have been recognized as the primary tool for past and future climate simulations and impact assessments (Abatzoglou et al., 2019; Deng et al., 2021; Jain et al., 2022; Vautard et al., 2014). Recent activities associated with the Coupled Model Intercomparison Project (CMIP) have demonstrated that a multi-model framework contributes to a more robust understanding of the Earth system and its processes. The CMIP Phase 3 (CMIP3) simulations were used to prepare the fourth assessment report of the Intergovernmental Panel on Climate Change (IPCC) (Solomon et al., 2007). The CMIP Phase 5 (CMIP5) simulations included more than 40 GCMs and used a new set of emission scenarios named Representative Concentration Pathways (RCP). Substantial improvements of participant GCMs in CMIP5 produced valuable climate information for policymakers and the scientific community (Stocker et al., 2013; Taylor et al., 2012). The latest phase of CMIP, CMIP6, includes internationally coordinated experiments of global climate modeling designed to provide insight into different climate responses and mechanisms. The models in CMIP6 generally have finer resolution with improved dynamic processes, and the new Shared Socioeconomic Pathway (SSP)-based scenarios are applied for future climate change simulations (O'Neill et al., 2016). CMIP6 plays an important role in international Earth system science and is a key IPCC assessment activity (Masson-Delmotte et al., 2021).

The scientific community must quantify the spatial heterogeneity of climate change in order to identify where, and to what extent, lives and livelihoods will be at risk in the future, and to facilitate actionable adaptation and mitigation plans. The native spatial resolution of the CMIP GCM simulations is too coarse to achieve these goals, but efforts to downscale climate projections have led to better understanding of finer scale patterns of change (Navarro-Racines et al., 2020; Pierce et al., 2014; Thrasher et al., 2012; Vandal et al., 2017). Furthermore, systematic biases in GCM simulations often hamper the accurate assessment of climate change projection (Hempel et al., 2013; Thrasher et al., 2012). NASA Earth eXchange Global Daily Downscaled Projections (NEX-GDDP, https://www.nasa.gov/nex/gddp) is one of the downscaling and bias-correction efforts, and has provided a bias-corrected, high-resolution, and seamless daily climate projections from both CMIP5 and CMIP6 (Thrasher et al., 2022).

In this study, we leverage the recent release of the NEX-GDDP-CMIP6 data set (Thrasher et al., 2022) to understand how different regions will be affected by climate at 2°C of global warming. We first identify the time when global mean temperature reaches +2°C compared to the pre-industrial period (1850–1900), termed the "crossing year." Then we investigate how temperature, precipitation, relative humidity, radiation, and wind speed have changed at the crossing year compared to a baseline period (1950–1979). In addition to the key climate variables, we also investigate two important climate impact indicators, fire weather index (FWI) (Van Wagner & Forest, 1987) and wet bulb global temperature (WBGT) (Lemke & Kjellstrom, 2012). These indicators allow us to gauge risks of fire and heat stress in the crossing year. By doing so, we provide a unique assessment of what the 2°C goal might mean for the global land climate, overall and across regions, and how this compares to the global average.

2. Materials and Methods

2.1. NEX-GDDP-CMIP6

The NEX-GDDP-CMIP6 data sets contain downscaled climate projections derived from the CMIP6 GCM simulations with four SSP scenarios: SSP1-2.6, SSSP2-4.5, SSP3-7.0, and SSP5-8.5. The spatial resolution of the data set is 0.25° × 0.25° (~25 × 25 km). These datasets provide a set of global, bias-corrected, high-resolution, and seamless daily climate projection over land for the period from 1950 through 2014 (retrospective run) and from 2015 to 2100 (prospective run) by combining ground observations and native GCM results (Thrasher et al., 2022). It improves CMIP6 simulations from large scale to regional-to-local scales with an unchanged long-term trend (Thrasher et al., 2012). Each downscaled climate projection includes nine climate variables (see Thrasher et al. (2022) for details). In this study, we use all 35 NEX-GDDP-CMIP6 GCMs and focus on six key climate variables: mean near-surface air temperature (*tas*), precipitation (*pr*), near-surface relative humidity (*hurs*), surface downwelling radiation (shortwave: *rsds*, longwave: *rlds*), and near-surface wind speed (*sfcWind*) (Table 1). Two future SSP scenarios are considered in this study: SSP2-4.5 and SSP5-8.5 (O'Neill et al., 2016).

23284277, 2023, 5, Downloaded from https://agupubs.onlinelibrary.wiley.com/doi/10.1029/2022EF003330 by NASA Shared Services Center (NSSC), Wiley Online Library on [08/03/2024]. See the Terms and Conditions (https://onlinelibrary.wiley.com/terms-and-conditions) on Wiley Online Library for rules of use; OA articles are governed by the applicable Creative Commons License

23284277, 2023, 5, Downloaded from https://agupubs.onlinelibrary.wiley.com/doi/10.1029/2022EF003330 by NASA Shared Services Center (NSSC), Wiley Online Library on [08/03/2024]. See the Terms and Conditions (https://onlinelibrary.wiley.com/terms-and-conditions) on Wiley Online Library for rules of use; OA articles are governed by the applicable Creative Commons License

Table 1
Description of NASA Earth eXchange Global Daily Downscaled Projections -CMIP6 Data Used in This Study

	NEX-GDDP-CMIP6
Model	Total 35 models: ACCESS-CM2, ACCESS-ESM1-5, BCC-CSM2-MR, CanESM5, CESM2, CESM2-WACCM, MCC-CM2-SR5, CMCC-ESM2, CNRM-CM6-1, CNRM-ESM2-1, EC-Earth3, EC-Earth3-Veg-LR, FGOALS-g3, GFDL-CM4 (gr1), GFDL-CM4 (gr2), GFDL-ESM4, GISS-E2-1-G, HadGEM3-GC31-LL, HadGEM3-GC31-MM, IITM-ESM, INM-CM4-8, INM-CM5-0, IPSL-CM6A-LR, KACE-1-0-G, KIOST-ESM, MIROC-ES2L, MIROC6, MPI-ESM1-2-HR, PI-ESM1-2-LR, MRI-ESM2-0, NESM3, NorESM2-LM, NorESM2-MM, TaiESM1, UKESM1-0-LL
Simulation	Historical (1950–2014)
	SSP2-4.5 (2015–2100)
	SSP5-8.5 (2015–2100)
Variable	*hurs*[a], *pr*[b], *rlds*[c], *rsds*[d], *sfcWind*[e], *tas*[f]
Temporal Coverage	1950-01-01–2100-12-31
Temporal Resolution	Daily
Spatial Resolution	0.25° × 0.25°

[a]Near-surface relative humidity (%). [b]Precipitation (mm/year). [c]Surface downwelling longwave radiation (W/m^2). [d]Surface downwelling shortwave radiation (W/m^2). [e]Near-surface wind speed (m/s). [f]Mean near-surface air temperature (°C).

SSP5-8.5 represents an extreme scenario (also called "Fossil-fueled Development: Taking the Highway") in which no policies are applied regarding the emission of greenhouse gasses, that is, with intensive fossil-fuel consumption resulting in a forcing pathway of 8.5 W/m^2 in 2100. SSP2-4.5 is an intermediate scenario (also called "Middle of the Road"), in which current climate change trends continue without substantial deviations, leading to a forcing pathway of 4.5 W/m^2 by 2100.

2.2. Detection of the +2°C Crossing Year

This study defines the +2°C crossing year as the time when the running 30-year average global mean near-surface air temperature reaches +2°C compared to a pre-industrial period (1850–1900). To define the +2°C period, we analyze past observed and projected temperatures. The following global observational data set has been analyzed for this purpose: HadCRUT (version 5.0.1.0) covering a period of 1850–2021 (Morice et al., 2021). We choose HadCRUT as other observational data sets (e.g., NASA GISS and NOAA NCDC) only cover from 1880. We use the 30 years between 1950 and 1979 as the baseline period in calculating climate changes. The warming from the preindustrial era to the baseline period is estimated to be 0.25°C based on the HadCRUT data set. We then use annual mean temperatures from multimodel ensemble median (MME) of native CMIP6 (35 GCMs) datasets (1950–2100) to detect the year when an additional +1.75°C from the baseline period is reached. This year is defined as the +2°C crossing year. Note that we use the native CMIP6 data instead of NEX-GDDP-CMIP6 in the crossing year detection to fully consider temperature changes over ocean and land areas in defining global 2°C warming. In addition to the global scale crossing year retrieval from MME, we also detect individual GCM based crossing year retrievals to evaluate the degree of variability in the crossing year among the GCMs.

2.3. Quantification of Projected Changes in Key Climate Variables and Impact Indicators

This study identifies the decade when the detected +2°C crossing year from both individual and MME of native CMIP6 models mostly falls in. We then use NEX-GDDP-CMIP6 data to quantify changes in climate conditions of the identified decade with respect to the baseline period (1950–1979). Changes in projected climates under two different SSP scenarios, SSP2-4.5 and SSP5-8.5, are investigated. Six different climate variables used in this study include mean near-surface air temperature (*tas*), precipitation (*pr*), near-surface relative humidity (*hurs*), surface downwelling radiation (shortwave: *rsds*, longwave: *rlds*), and near-surface wind speed (*sfcWind*). Furthermore, we use two important climate impact indicators, FWI and WBGT, to assess risks of fire and heat stress under projected climates in the identified decade for +2°C crossing year. For the sake of simplicity, we only

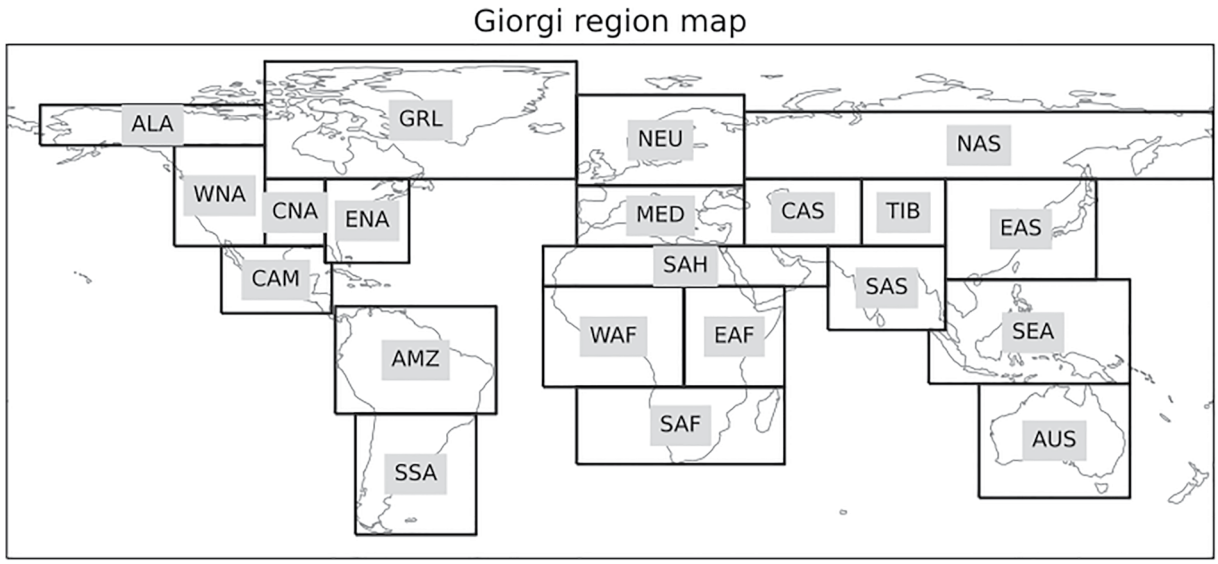

Figure 1. Map of regions defined by "Giorgi Regions." These regions are used to compute the regional variation of NASA Earth eXchange Global Daily Downscaled Projections climate variables. Each abbreviation stands for a region, that is, AUS, Australia; AMZ, Amazon; SSA, Southern South America; CAM, Central America; WNA, Western North America; CNA, Central North America; ENA, Eastern North America; ALA, Alaska; GRL, Greenland; MED, Mediterranean; NEU, Northern Europe; WAF, Western Africa; EAF, Eastern Africa; SAF, Southern Africa; SAH, Sahara; SEA, Southeast Asia; EAS, East Asia; SAS, South Asia; CAS, Central Asia; TIB, Tibet; NAS, North Asia.

provide a short description of each indicator here. Details of calculating FWI (Van Wagner & Forest, 1987) and WBGT (Lemke & Kjellstrom, 2012) can be found in the corresponding references.

FWI is a meteorologically based index used widely to estimate fire danger under given weather conditions (Van Wagner & Forest, 1987). The FWI from the Canadian Forest Fire Weather Index System is used in this study given its widespread usage globally (Abatzoglou et al., 2019; Di Giuseppe et al., 2016). The system was originally developed as a numerical proxy for fire behavior in evergreen forests of eastern Canada, but has been shown to be an effective correlate of intraseasonal to interannual fire activity across diverse vegetation types (Abatzoglou et al., 2019). It consists of various sub-components (fine fuel moisture code, duff moisture code, drought code, initial spread index, build up index, and fire weather index) that account for the effects of fuel moisture and wind on fire behavior and spread. Detailed descriptions of the sub-components can be found in Supporting Information S1 Method. Higher FWI values correspond to more favorable meteorological conditions for wildfires. To analyze how the distribution of extreme fire weather changes through time, we compute the annual 95th percentile of the FWI (FWI_{P95}, hereafter). We also count the number of days that exceed a critical daily FWI condition (FWI > 30, Fargeon et al., 2020) throughout a year and use it as another indicator (FWI_{N30}) for the annual fire danger index.

We compute sWBGT, a simplified version of WBGT, using the NEX-GDDP-CMIP6 data set (Lemke & Kjellstrom, 2012). The sWBGT is a combined measure of temperature and humidity effects on thermal comfort that has been widely used to define heat stress on public health (Alves de Oliveira et al., 2021; Raymond et al., 2020). According to previous studies and public health guidelines, when sWBGT is greater than 28, the danger of heat disorders is high so any kinds of daily activities may lead to severe health risk (e.g., Asayama, 2009). We calculate the annual 95th percentile of the sWBGT ($sWBGT_{P95}$) and the number of days ($sWBGT_{N28}$) that exceed a critical daily sWBGT condition (sWBGT > 28) throughout a year. We use them as indicators for the annual heat stress index.

We analyze key results based on NEX-GDDP-CMIP6 SSP2-4.5 with a comparison to SSP5-8.5 and summarize them by the regions defined in Figure 1 (Giorgi & Francisco, 2000).

23284277, 2023, 5, Downloaded from https://agupubs.onlinelibrary.wiley.com/doi/10.1029/2022EF003330 by NASA Shared Services Center (NSSC), Wiley Online Library on [08/03/2024]. See the Terms and Conditions (https://onlinelibrary.wiley.com/terms-and-conditions) on Wiley Online Library for rules of use; OA articles are governed by the applicable Creative Commons License

10.1029/2022EF003330

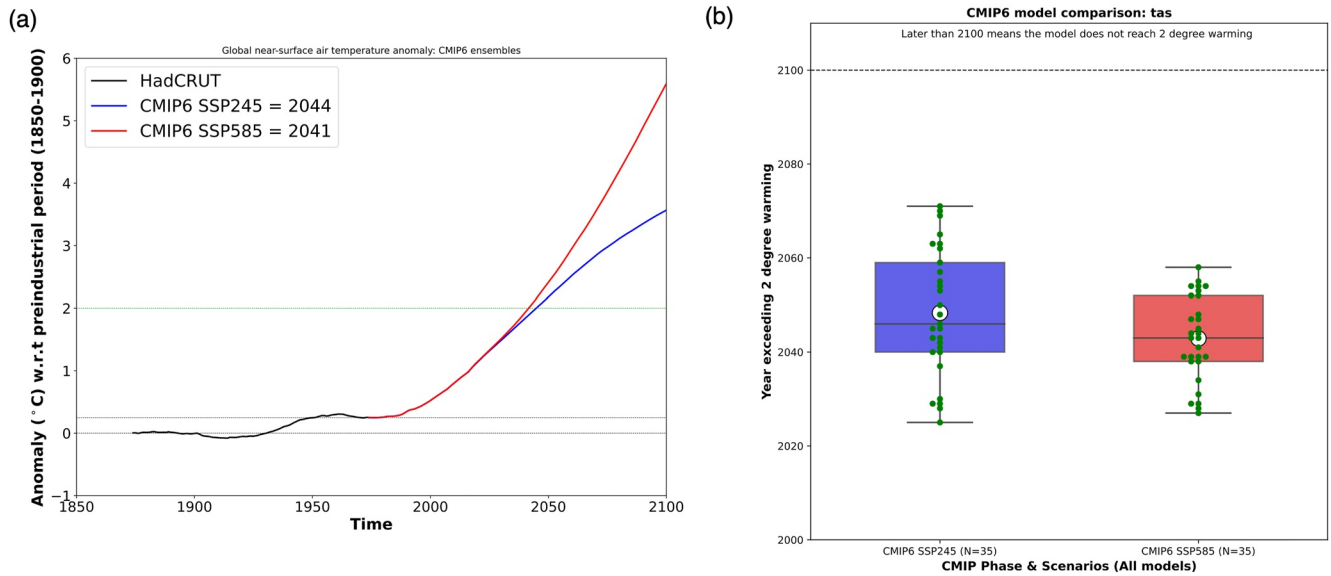

Figure 2. (a) Time series of running 30-year average global mean near-surface air temperature of CMIP6 (blue: SSP2-4.5, red: SSP5-8.5) multi-model ensemble median. Green horizontal line shows 2°C warming with respect to a baseline period (1950–1979) and detected crossing years are shown in the legend box. (b) Distribution of year exceeding 2°C degree warming across CMIP6 (SSP2-4.5 & SSP5-8.5) General circulation models (GCMs) under different scenarios. Each green dot represents individual GCMs of CMIP6. Note that dots greater than 2,100 mean that the models do not project +2°C warming until the end of 21st century.

3. Results and Discussion

3.1. Year Crossing 2°C Warming

Figure 2a illustrates the time that global average near-surface air temperature reaches 2°C warming with respect to the pre-industrial period (1850–1900). The higher emission scenario (SSP5-8.5) in CMIP6 shows a faster rate of temperature increase during the 21st century. The detected crossing year of CMIP6 MME under the higher emission scenarios (SSP5-8.5) is 2041, while simulations under the lower emission scenario (SSP2-4.5) indicate a later crossing year (2044). The projected crossing year from individual CMIP6 GCMs shows considerable spread ranging from 2025 to 2071 (median = 2048) and from 2027 to 2058 (median = 2043) under SSP2-4.5 and SSP5-8.5, respectively (Figure 2a, see Texts and Figure S1 in Supporting Information S1 for the crossing year retrievals from CMIP5 GCMs). Based on the analysis of crossing year detection, we keep the 2040s as a base period to demonstrate the projected climate change in the following sections as the central estimates of the time crossing the 2°C threshold of all CMIP phases and scenarios lie in the 2040s (Figure 2 & Figure S1 in Supporting Information S1).

3.2. Near-Surface Air Temperature

In the 2040s, global mean near-surface air temperature over land is projected to increase by 2.33°C and 2.79°C under the SSP2-4.5 and SSP5-8.5 scenarios, respectively (Figure 3a). The projected changes over land are higher than 2°C as oceans warm less rapidly so that GCMs project more warming over land than the ocean (Sutton et al., 2007). Divergence of temperature changes between the two scenarios significantly increases after the 2040s, whereas only a small difference exists between the two SSPs in the 2040s, indicating minor scenario dependence in near-term projections. Significant polar region warming known as "*Arctic amplification*" is noticeable in the high latitude regions including Alaska, Canada, Northern Europe, and Russia (Serreze & Barry, 2011) (Figures 3b and 3c). In particular, Greenland, Alaska, and North Asia are projected to reach a >3°C increase in annual temperature by the 2040s. South Asia, Eastern and Western Africa, and Southern South America show a relatively lower rate of temperature change. Relative changes in near-surface air temperature show similar geographical patterns with the absolute change emphasizing a greater warming in high latitude regions (Figure S2 in Supporting Information S1). As anticipated, the projected temperature changes under SSP5-8.5 are greater than those under the SSP2-4.5 scenario. High latitude regions reveal a greater difference in the projected temperature changes (>0.4°C) between the two SSPs, suggesting an accelerated warming over polar regions with positive

23284277, 2023, 5, Downloaded from https://agupubs.onlinelibrary.wiley.com/doi/10.1029/2022EF003330 by NASA Shared Services Center (NSSC), Wiley Online Library on [08/03/2024]. See the Terms and Conditions (https://onlinelibrary.wiley.com/terms-and-conditions) on Wiley Online Library for rules of use; OA articles are governed by the applicable Creative Commons License

10.1029/2022EF003330

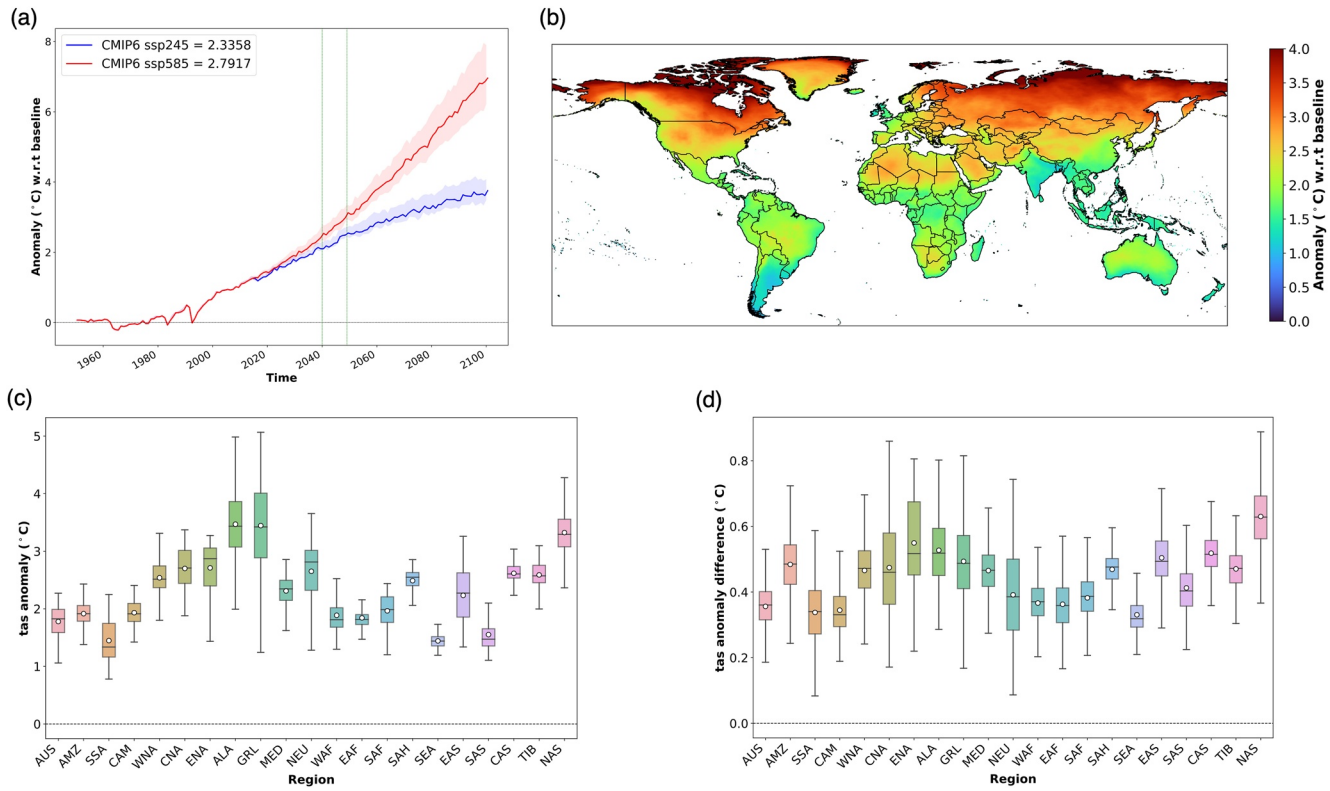

Figure 3. (a) Multimodel ensemble median (MME) time series of near surface air temperature in historical (1950–2014) and future (2015–2100) scenarios, that is, SSP2-4.5 (blue) and SSP5-8.5 (red), are shown relative to the baseline period (1950–1979). Shaded area of each scenario shows a range of 25th and 75th percentile of multi-model projections. (b) Spatial pattern of MME of near surface air temperature anomaly (SSP2-4.5) in the 2040s with respect to the baseline. (c) Regional summary of changes in the near-surface air temperature anomaly (SSP2-4.5) shown in (b). (d) Regional summary of differences (SSP5-8.5 – SSP2-4.5) between anomalies of two scenarios. The box stretches from the 25th percentile to the 75th percentile of target regional data. The median and mean values are shown as a solid line and a hollow dot, respectively.

feedback (e.g., albedo, sea ice, cloud, and water vapor) under the higher emission scenario (Hahn et al., 2021) (Figure 3d).

3.3. Precipitation

In general, CMIP6 models show consistent increases in global precipitation since the 2000s, and its upward trend is projected to continue through the 21st century (Figure 4a). In the 2040s, ~13 and 20 mm/year more precipitation will be observable in the SSP2-4.5 and SSP8-5.8 scenarios respectively. Widespread precipitation increases over the northern hemisphere >50°N are projected in the near future. Southeastern Greenland shows a strikingly rapid increase in precipitation (Figures 4b and 4c). This increase over the high latitudes is likely dominated by rainfall, implying a transition from a snow-to rain-dominated high latitude region, especially in the summer and fall seasons (McCrystall et al., 2021). However, precipitation changes in the 2040s show a contrasting pattern in the tropics. Over the Amazon basin, annual precipitation will decrease by ~98 mm/year. Dry regions, including Southern Africa, Southwest North America, Australia, Sahel, and Mediterranean regions, also show a widespread decline in precipitation in the 2040s. In contrast, Western (+82 mm/year) and Eastern (+52 mm/year) Africa and South Asia (+64 mm/year) show a remarkable increase in precipitation in the SSP2-4.5 projection. Significant relative changes in precipitation with respect to the baseline emerge over high Arctic, Sahel, and Northern Africa (Figure S3 in Supporting Information S1). There is observational evidence of recent increase in precipitation over southern Sahel (e.g., Panthou et al., 2018) and it is strongly associated with the surface warming over northern Africa, which favors the displacement of the monsoon northwards (Park et al., 2015). In the higher emission scenario, the contrasting pattern of precipitation changes over the tropics is strengthened: more precipitation over Western/Eastern Africa and South/Southeast Asia whereas less precipitation over the Amazon (Figure 4d). The "*wet get wetter*, *dry get drier*" paradigm, that has been used to explain

23284277, 2023, 5, Downloaded from https://agupubs.onlinelibrary.wiley.com/doi/10.1029/2022EF003330 by NASA Shared Services Center (NSSC), Wiley Online Library on [08/03/2024]. See the Terms and Conditions (https://onlinelibrary.wiley.com/terms-and-conditions) on Wiley Online Library for rules of use; OA articles are governed by the applicable Creative Commons License

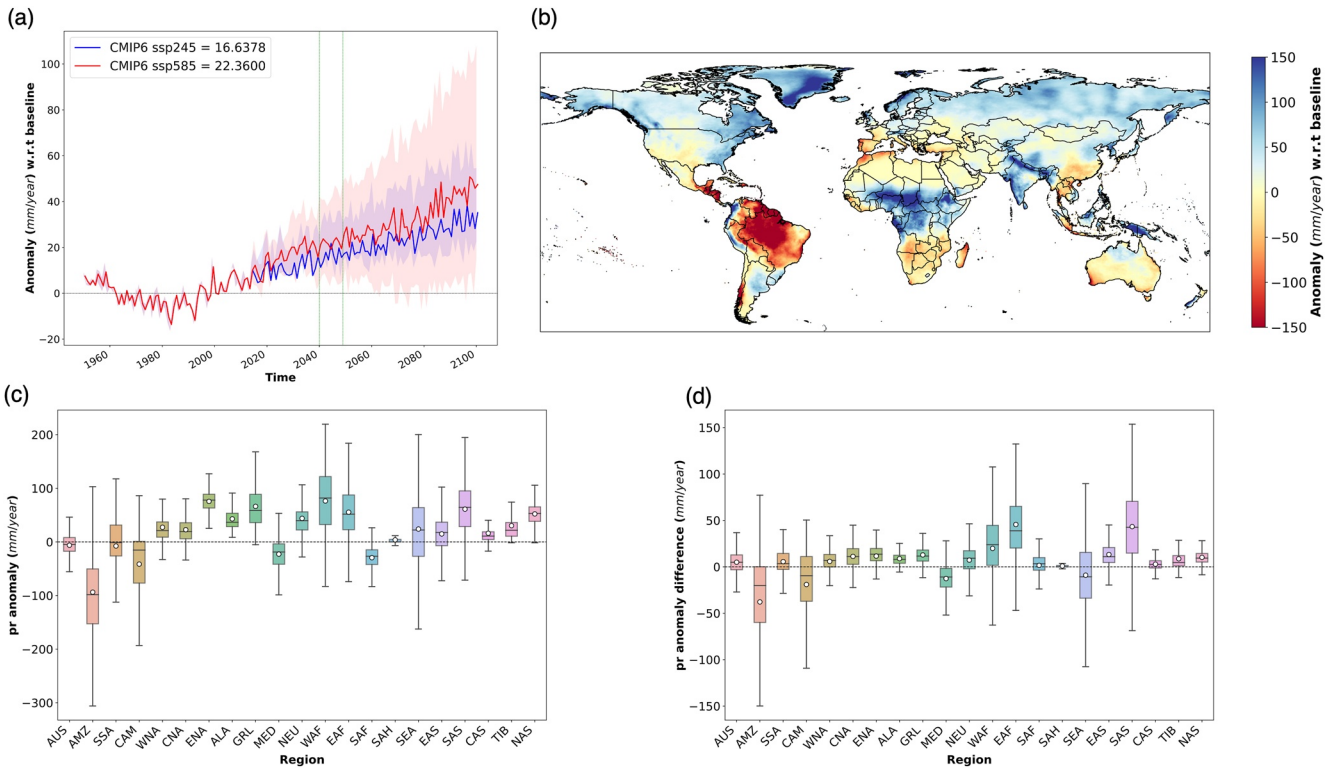

Figure 4. Same as Figure 3 but for precipitation (pr).

the global precipitation pattern responding to global warming, may not hold, especially over tropical regions in the Amazon and Southeast Asia where "*wet gets drier*" patterns are projected (Greve et al., 2014). The projected rainfall decline in the Amazon has been linked to changes in the tropical Pacific (Parsons, 2020) and the response of vegetation to elevated CO_2 (Richardson et al., 2018).

3.4. Relative Humidity

Relative humidity is the amount of moisture in the air (via moisture mass or vapor pressure) divided by the maximum amount of moisture that could exist in the air at a specific temperature (via max moisture mass or saturation vapor pressure). This quantity is critical in many perspectives such as climate, air quality, human comfort/health/industry, etc. At the global scale, relative humidity is projected to decrease by 0.62% and 0.73% in the 2040s under SSP2-4.5 and SSP5-8.5 scenarios respectively (Figure 5a). Most global land areas except Western (+0.65%)/Eastern Africa (+0.68%) and South Asia (+1.83%) where increasing precipitation is projected show a increasing pattern of relative humidity (Figures 5b and 5c). The most significant decrease of relative humidity is found in the Amazon (−1.7%), particularly over the southeastern edge of the rainforests called the "*Arc of Deforestation*," where extensive land cover/use changes are happening. Central North America and Mediterranean regions also display significant decreases in relative humidity. The decrease in relative humidity over most land areas is associated with the larger warming rates over land and is attributable to the last-saturation-temperature constraint (Denson et al., 2021). Similar geographical patterns of relative changes in humidity during the 2040s are projected (Figure S4 in Supporting Information S1). In the SSP5-8.5 scenario, the projected decrease and increase in regional relative humidity are more dramatic (Figure 5d). For instance, Amazon and Western/Eastern Africa under SSP5-8.5 will get lower and higher relative humidity than the ones from SSP2-4.5 respectively.

3.5. Radiation

The CMIP6 hindcast for global downwelling shortwave radiation shows a rapid decrease during the period from 1950 to 2014 (Figure 6a), and captures abrupt but transient strong reductions during the 1960, 1980, and 1990s

23284277, 2023, 5, Downloaded from https://agupubs.onlinelibrary.wiley.com/doi/10.1029/2022EF003330 by NASA Shared Services Center (NSSC), Wiley Online Library on [08/03/2024]. See the Terms and Conditions (https://onlinelibrary.wiley.com/terms-and-conditions) on Wiley Online Library for rules of use; OA articles are governed by the applicable Creative Commons License

10.1029/2022EF003330

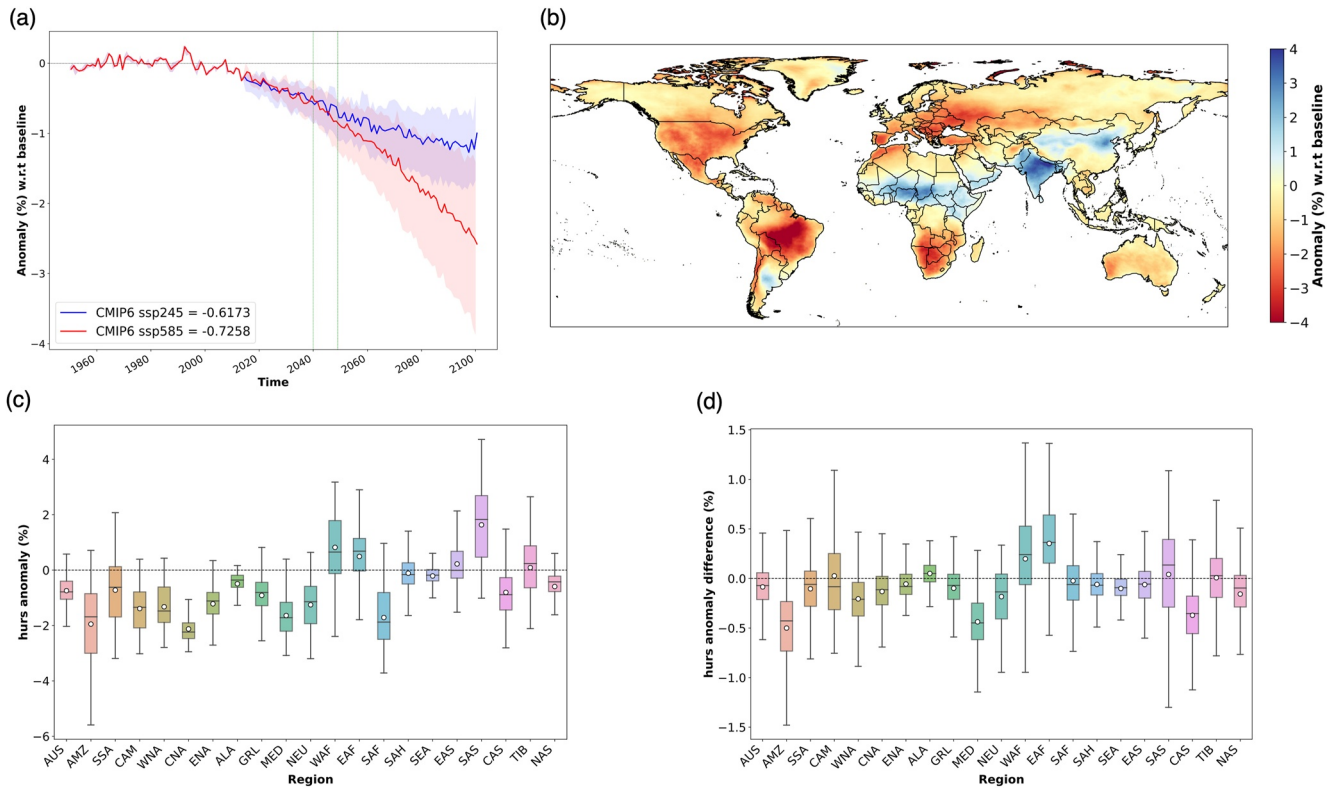

Figure 5. Same as Figure 3 but for near-surface relative humidity (hurs).

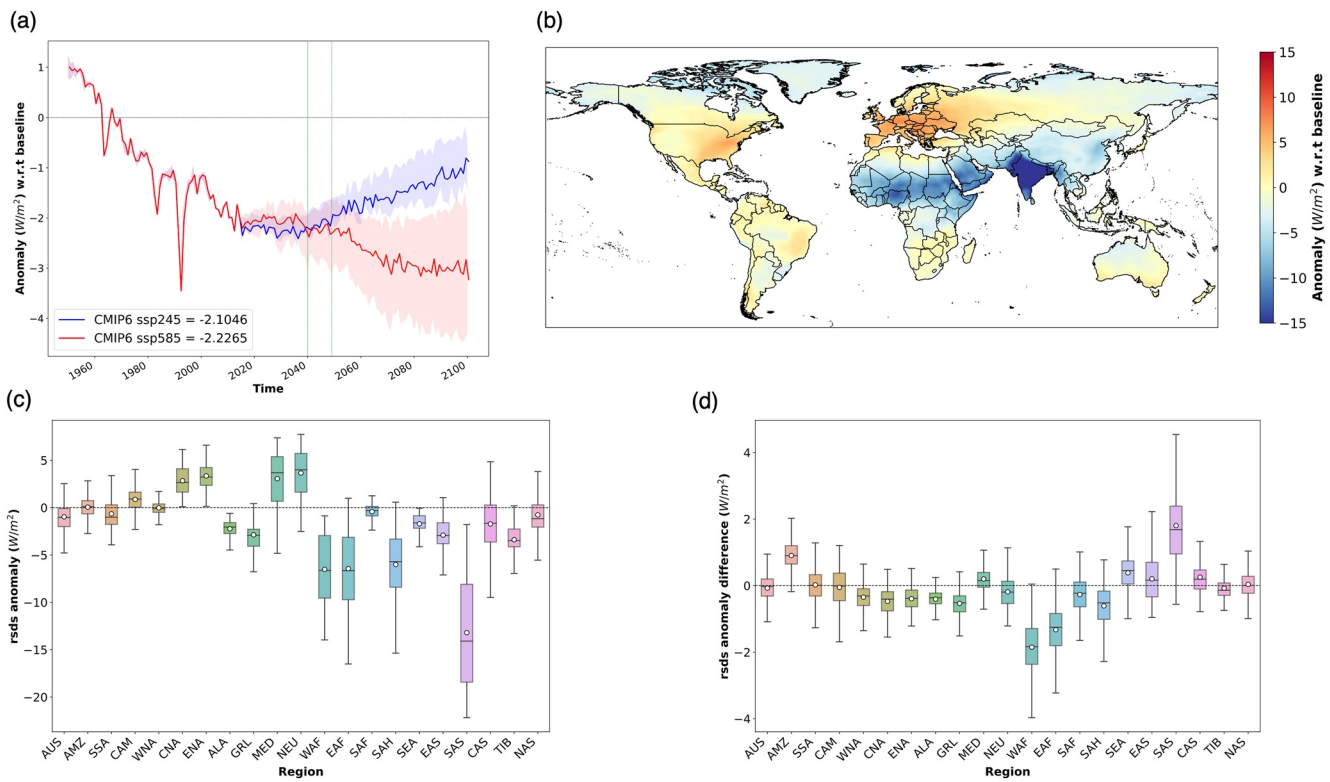

Figure 6. Same as Figure 3 but for surface downwelling shortwave radiation (rsds).

23284277, 2023, 5, Downloaded from https://agupubs.onlinelibrary.wiley.com/doi/10.1029/2022EF003330 by NASA Shared Services Center (NSSC), Wiley Online Library on [08/03/2024]. See the Terms and Conditions (https://onlinelibrary.wiley.com/terms-and-conditions) on Wiley Online Library for rules of use; OA articles are governed by the applicable Creative Commons License

10.1029/2022EF003330

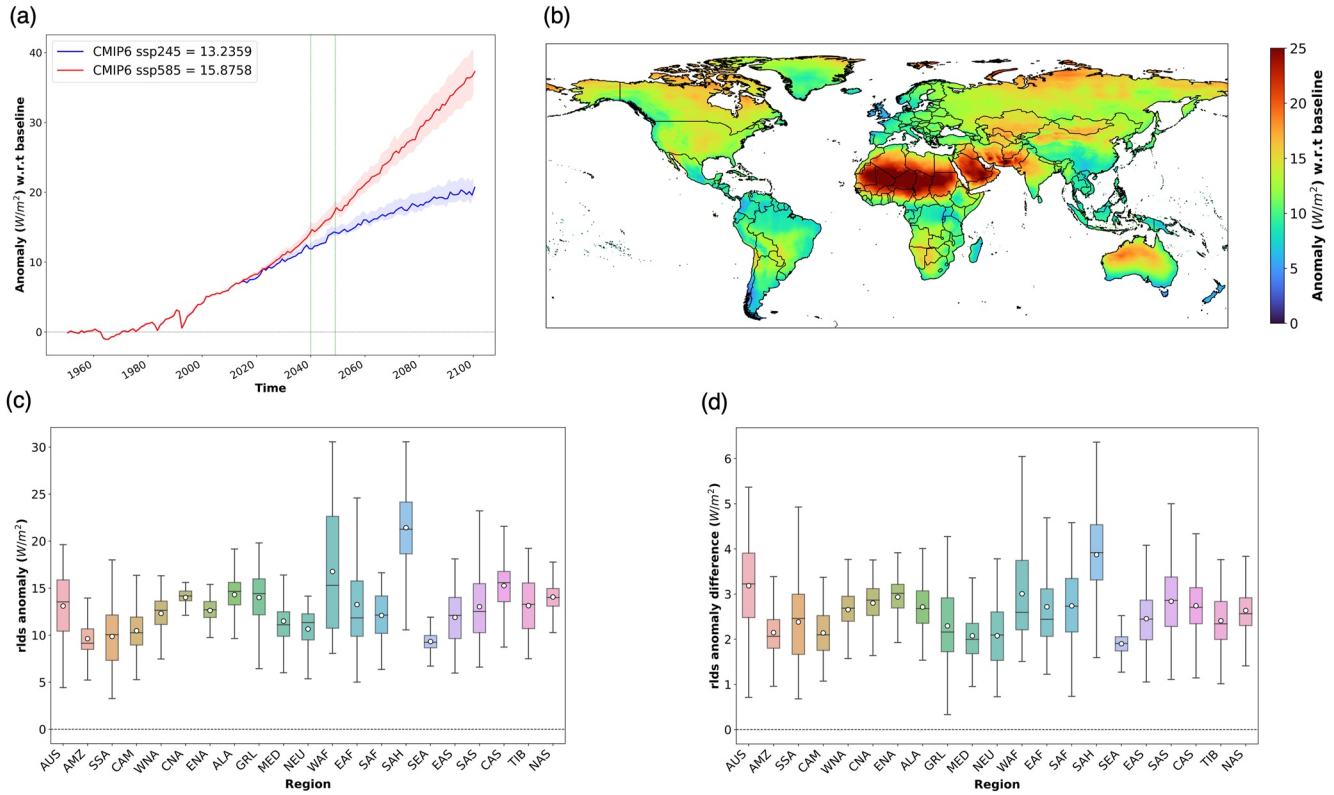

Figure 7. Same as Figure 3 but for surface downwelling longwave radiation (rlds).

due to large volcanic eruptions of Mount Agung (March 1963), El Chichón (April 1982), and Mount Pinatubo (June 1991) (Kirchner et al., 1999). Projected changes under two scenarios reveal divergent trends during the rest of the 21st century: a hiatus for four decades (2015–2055), then an upward trend for SSP2-4.5 and a downward trend for SSP5-8.5. This rebounding pattern is likely due to a reduction in aerosol burden under the moderate emission scenario (Westervelt et al., 2015). In the 2040s, downwelling shortwave radiation under SSP2-4.5 scenario is projected to decrease by ∼2.1 W/m^2. The Sahel (−5.7 W/m^2), Western/Eastern Africa (−6.6 W/m^2), and South Asia (−14.1 W/m^2) are where the most significant reduction of downwelling shortwave radiation is projected (Figures 6b and 6c). The Mediterranean (+3.7 W/m^2), Northern Europe (+4.0 W/m^2), and Eastern North America (+3.2 W/m^2) show increasing shortwave radiation in the 2040s. The projected relative changes show a generally consistent pattern with the absolute change (Figure S5 in Supporting Information S1). Compared to SSP2-4.5, the SSP5-8.5 simulation shows a slight increase generally, but South Asia (+1.7 W/m^2) and Amazon (+0.9 W/m^2) show significant increases whereas Western (−1.9 W/m^2) and Eastern (−1.8 W/m^2) Africa shows strong decreases (Figure 6d).

In contrast to shortwave radiation, surface downwelling longwave radiation has gradually increased during the hindcast period (1950–2014) and is projected to continue its upward trend in the rest of the 21st century (Figure 7a). In the 2040s, ∼13.2 and 15.9 W/m^2 of increase are projected under SSP2-4.5 and SSP5-8.5 scenarios, and divergence between the two scenarios likely gets larger in the later period of the century. A large increase is observed over the Sahel (+21.3 W/m^2) and Western Africa (+15.3 W/m^2) (Figures 7b and 7c), while relatively smaller projected changes are observed in the Amazon (+9.1 W/m^2), Southeast Asia (+9.2 W/m^2), and Southern South America (+10.1 W/m^2). The projected relative changes show a generally consistent pattern with the absolute change but reveal large increases over high latitude regions including Greenland, Northern Asia, and Alaska (Figure S6 in Supporting Information S1). In the SSP5-8.5 scenario, most regions are expected to experience a further increase of ∼2 W/m^2 in the 2040s compared to SSP2-4.5 (Figure 7d).

23284277, 2023, 5, Downloaded from https://agupubs.onlinelibrary.wiley.com/doi/10.1029/2022EF003330 by NASA Shared Services Center (NSSC), Wiley Online Library on [08/03/2024]. See the Terms and Conditions (https://onlinelibrary.wiley.com/terms-and-conditions) on Wiley Online Library for rules of use; OA articles are governed by the applicable Creative Commons License

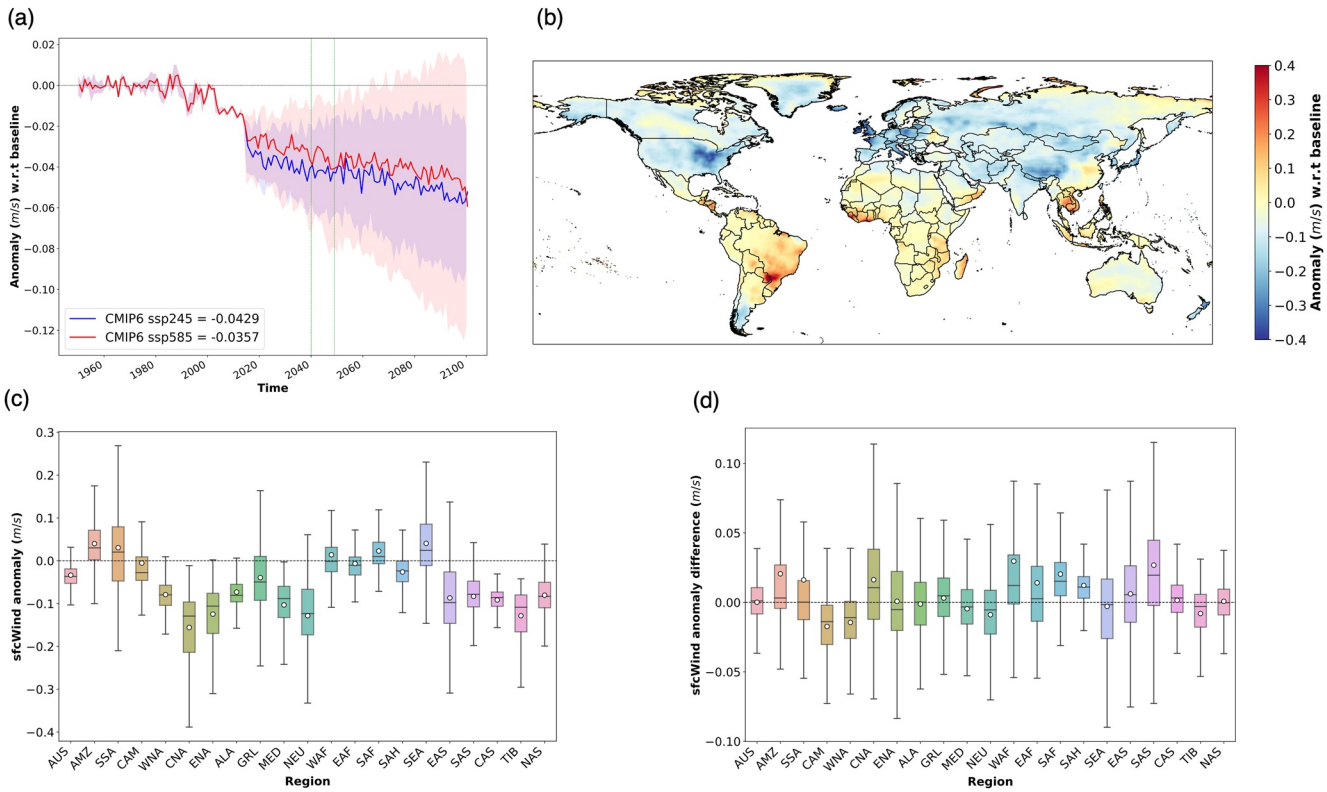

Figure 8. Same as Figure 3 but for near-surface wind speed (sfcWind).

3.6. Wind Speed

Global wind speed abruptly decreases during the period between the 1990 and 2020s, and this trend is projected to continue over the rest of the 21st century with a smaller rate of change (Figure 8a). This weakened wind speed over land is known as "terrestrial stilling", and it has been reported globally (Deng et al., 2021; McVicar et al., 2012). There are two major drivers of terrestrial stilling: (a) changes in large scale atmospheric circulation (Lu et al., 2007), and (b) an increase of surface roughness due to vegetation growth, land use/cover changes, and urbanization (Vautard et al., 2010). The CMIP6 GCMs are able to reproduce decreasing wind speed patterns over land during the historical period. In the 2040s, the CMIP6 models project that wind speed will decrease by 0.04 and 0.03 m/s under the SSP2-4.5 and SSP8-5.8 scenarios respectively. The most northern extratropic shows decreasing wind speed, whereas an increasing pattern is observable in most of the Southern Hemisphere (Figures 8b and 8c). A strong decrease of wind speed over Central (−0.13 m/s) and Eastern (−0.11 m/s) North America, Northern Europe (−0.12 m/s), and Tibet (−0.11 m/s) is noteworthy. We also find that the Amazon (+0.03 m/s) and Southeast Asia (+0.02 m/s) are projected to experience much windier conditions in the 2040s compared to the baseline. The projected wind speed decline over the Amazon and Southeast Asia are more evident when converted to a relative scale (Figure S7 in Supporting Information S1). Compared to SSP2-4.5, SSP5-8.5 shows less decline of wind speed over most global land areas except Central and Eastern North America, and Northern Europe (Figures 8a and 8d). The projected decreasing trends in wind speed indicate that terrestrial stilling will continue during the 21st century (Chen et al., 2021). However, there are studies reporting a reversal of wind speed change in the 2010s from observational records (Zeng et al., 2019), urging a comprehensive evaluation of the climate model projections.

3.7. Heat Stress

Projected key climate variables are expected to lead drastic changes in global heat stress on human health. Our analysis shows a robust upward trend in global $sWBGT_{P95}$ implying a higher extreme heat level during the 21st century (Figure 9a). Under the SSP2-4.5 and SSP5-8.5 scenarios, $sWBGT_{P95}$ during the 2040s is projected to

23284277, 2023, 5, Downloaded from https://agupubs.onlinelibrary.wiley.com/doi/10.1029/2022EF003330 by NASA Shared Services Center (NSSC), Wiley Online Library on [08/03/2024]. See the Terms and Conditions (https://onlinelibrary.wiley.com/terms-and-conditions) on Wiley Online Library for rules of use; OA articles are governed by the applicable Creative Commons License

10.1029/2022EF003330

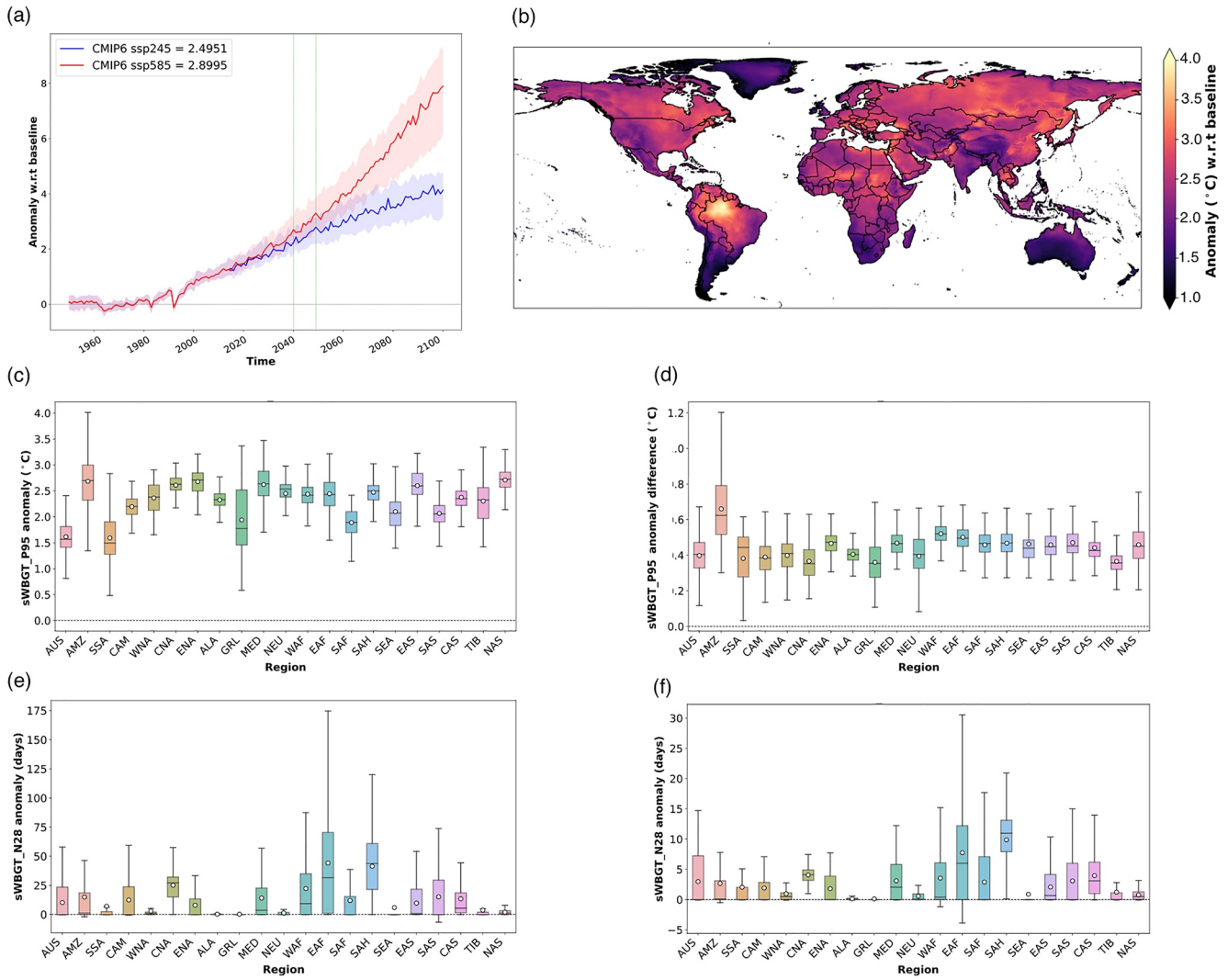

Figure 9. (a) Multimodel ensemble median (MME) time series of $sWBGT_{P95}$ in historical (1950–2014) and future (2015–2100) scenarios, that is, SSP2-4.5 (blue) and SSP5-8.5 (red), are shown relative to the baseline period (1950–1979). Shaded area of each scenario shows a range of 25th and 75th percentile of multi-model projections. (b) Spatial pattern of MME of $sWBGT_{P95}$ anomaly (SSP2-4.5) in the 2040s with respect to the baseline. (c) Regional summary of changes in the $sWBGT_{P95}$ anomaly (SSP2-4.5) shown in (b). (d) Regional summary of differences (SSP5-8.5 minus SSP2-4.5) between anomalies of two scenarios. (e) Same as (c) but for $sWBGT_{N28}$. (f) Same as (d) but for $sWBGT_{N28}$. The box stretches from the 25th percentile to the 75th percentile of target regional data. The median and mean values are shown as a solid line and a hollow dot, respectively.

change by 2.5°C and 2.9°C with respect to the baseline (1950–1979) respectively. Most global lands will likely experience at least an increase of 2.0°C $sWBGT_{P95}$ in the 2040s (Figures 9b and 9c). Greater increases (>2.5°C) may happen over the Amazon, Central and Eastern North America, Mediterranean, and Eastern and Northern Asia, while Australia and South America may experience a lower degree of changes in extreme heat. Further heat stress under the higher emission scenario (SSP5-8.5) is evident and widespread: about 0.4 –0.5°C of additional increase in global $sWBGT_{P95}$ is projected (Figure 9d). Unlike the changing pattern in Figure 9b, relative changes in $sWBGT_{P95}$ with respect to the baseline show significant increases over high latitude (e.g., Greenland and Alaska) and altitude (e.g., Tibetan plateau) regions (Figure S8 in Supporting Information S1).

Like $sWBGT_{P95}$, most global regions are generally expected to have more days with extreme heat stress condition (i.e., $sWBGT_{N28}$) in the 2040s, especially Western North America (+27 days), Eastern Africa (+32 days), and Sahel (+44 days) (Figure 9e). However, the spatial patterns of changes in $sWBGT_{N28}$ are different from those of $sWBGT_{P95}$. In contrast to the widespread increase in $sWBGT_{P95}$, the projected increase of $sWBGT_{N28}$ is region-specific and mostly occurs in low latitude countries. These low latitude countries have disproportionately

23284277, 2023, 5, Downloaded from https://agupubs.onlinelibrary.wiley.com/doi/10.1029/2022EF003330 by NASA Shared Services Center (NSSC), Wiley Online Library on [08/03/2024]. See the Terms and Conditions (https://onlinelibrary.wiley.com/terms-and-conditions) on Wiley Online Library for rules of use; OA articles are governed by the applicable Creative Commons License

10.1029/2022EF003330

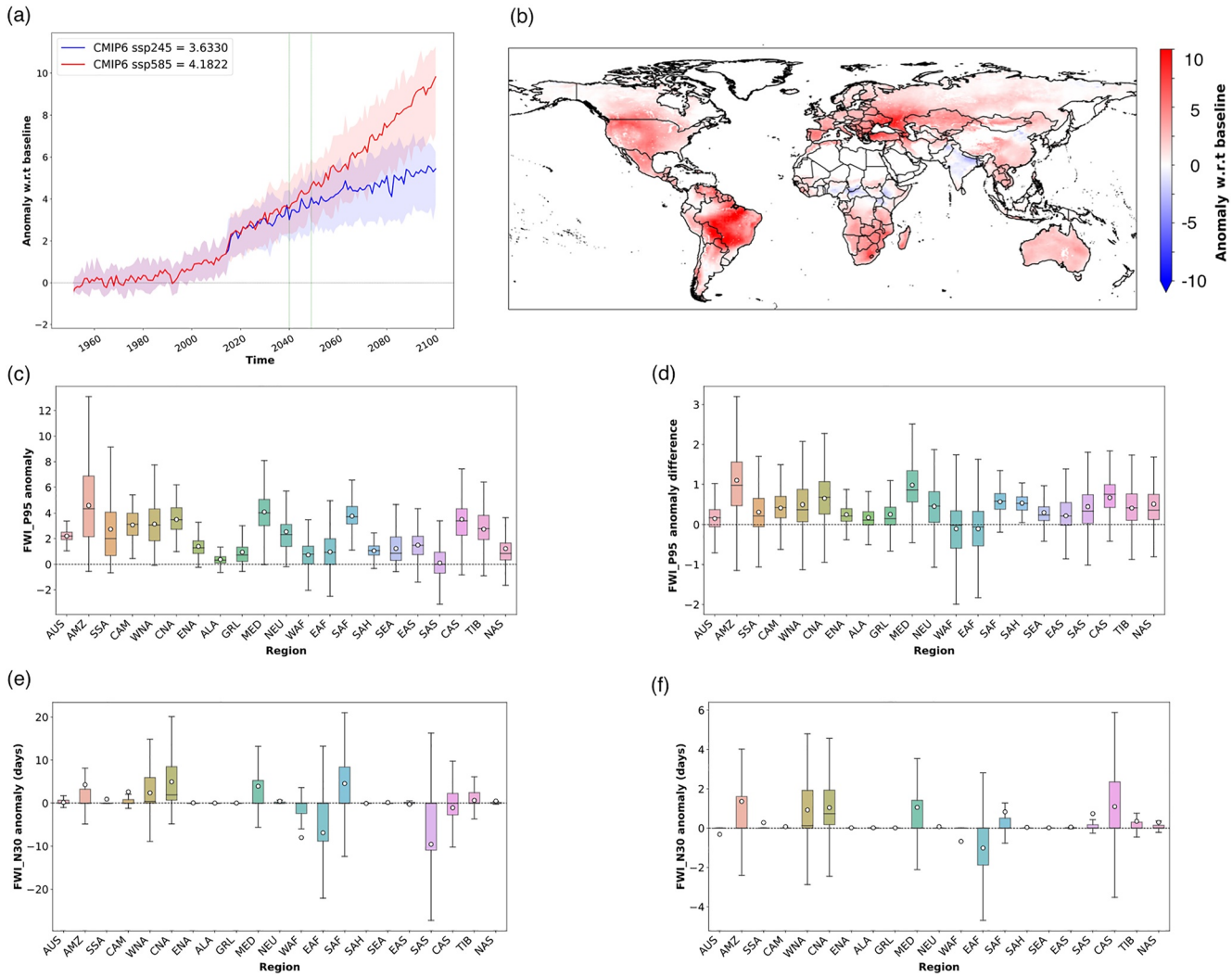

Figure 10. Same as Figure 9 but for FWI_{P95} and FWI_{N30}.

suffered from extreme heat events historically (Figure S2 in Supporting Information S1) and the higher emission scenario (SSP8-5.8) likely adds more days exceeding the heat stress threshold over most global land areas, especially over such low latitude regions (e.g., Africa) (Figure 9f). The exception in the high latitudes does not indicate that heat stress on such regions doesn't increase but it is insufficient for satisfying the higher sWBGT threshold condition.

3.8. Fire Weather

Changes in fire weather are functions of changes in temperature, precipitation, relative humidity, radiation, and wind speed suggesting a complex nature of FWI characterization. Time series of global mean FWI_{P95} indicate that the degree of extreme FWI conditions is projected to increase by 3.6 and 4.2 under SSP2-4.5 and SSP5-8.5 scenario compared to the baseline period (Figure 10a). Spatial pattern of FWI_{P95} varies significantly by ecoclimatic regions. Higher baseline FWI_{P95} is mostly observable over semi-arid ecosystems including Australia, Western North America, Northern and Southern Africa, South and Central Asia (Figure S4 in Supporting Information S1). The computed changes in FWI_{P95} under the moderate emission scenario (SSP2-4.5) reveals that Western and Central North America, Amazon, Mediterranean, and South Africa will be at higher risk of fire in the 2040s compared to the baseline period, whereas Eastern and Western Africa, and South Asia show a slight decrease or no change in FWI_{P95} (Figures 9b and 9c). This divergent regional pattern is strongly associated with

23284277, 2023, 5, Downloaded from https://agupubs.onlinelibrary.wiley.com/doi/10.1029/2022EF003330 by NASA Shared Services Center (NSSC), Wiley Online Library on [08/03/2024]. See the Terms and Conditions (https://onlinelibrary.wiley.com/terms-and-conditions) on Wiley Online Library for rules of use; OA articles are governed by the applicable Creative Commons License

23284277, 2023, 5, Downloaded from https://agupubs.onlinelibrary.wiley.com/doi/10.1029/2022EF003330 by NASA Shared Services Center (NSSC), Wiley Online Library on [08/03/2024]. See the Terms and Conditions (https://onlinelibrary.wiley.com/terms-and-conditions) on Wiley Online Library for rules of use; OA articles are governed by the applicable Creative Commons License

projected changes in precipitation as shown in Figure 4b revealing combined controls of climate variables on changes in FWI (Abatzoglou et al., 2019). More significant divergence is observable from FWI_{N30}. It is worthy to note that there is an exceptional increase of FWI_{N30} over Western and Central North America where historical fire frequency, size, and intensity have significantly increased during the last few decades (Abatzoglou & Williams, 2016). Another point to note is that northern boreal biomes and tropics are expected to experience a rapid relative change in FWI_{P95} and emerge as primary hotspots of future fire risk (Figure S9 in Supporting Information S1). Though it is highly uncertain whether regional fire activities will increase or not in future due to complex interactions between fire-human-climate-fuel systems (Riley et al., 2019), our analysis of FWI from 35 CMIP6 GCMs suggests that continued climate change will further elevate extreme fire risks (FWI_{P95} & FWI_{N30}) by the end of this century.

3.9. Other Potential Implications and Discussion

In addition to extreme heat stress, extreme precipitation events can cause substantial socio-economic damage by bringing cascading disasters (e.g., floods and landslides) (Madsen et al., 2014). The projected annual mean precipitation in the 2040s continuously increases in both moderate and high emission scenarios during the 21st century. In line with previous CMIP simulations, the CMIP6 simulations continue to project a large-scale picture of more frequent and more intense precipitation extremes under continued global warming (Almazroui et al., 2021). Changes in precipitation extremes follow changes in temperature globally at roughly the Clausius–Clapeyron rate of ~7%·°C^{-1} (C. Li et al., 2021), implying ~14% increase in extreme precipitation events (e.g., annual maximum 1-day (or 5-day) precipitation) at the 2°C warming crossing year period. Furthermore, a robust drought projection is also prominent over the global drylands of more frequent, intense, and longer duration (H. Li et al., 2021). These collectively reveal that extreme precipitation, heat, and drought events become more extreme and disastrous as Earth's climate warms, thus leading to escalating impacts of climate extremes.

The projected climate in the 2040s is also expected to change the potential of renewable energy resources such as wind, solar, and hydropower. Wind power density (P) is a function of wind speed (U) and air density (ρ), $P = 0.5 \cdot \rho \cdot U^3$ (Martinez & Iglesias, 2022). Due to the nature of the cubic relationship between P and U, small changes in wind speed result in large changes in wind power density. Our result shows that most mid- and high-latitude areas of the northern hemisphere, where most wind farms are currently operational or under construction, will have less wind power resources in near future, whereas the Amazon, Southern South America, Southeast Asia, and South America tend to get more wind power potential in the 2040s (Figure 8). The higher emission scenario likely increases the wind power density in the 2040s over most of the globe compared to the moderate emission scenario, though a large spread of future projections is noticeable. Like wind power resources, solar power potential for the concentrated Solar Power (CSP) plants or solar photovoltaic (PV) power also strongly depends on the solar radiation projection presented in Figure 6 (Dutta et al., 2022). Spatially varying magnitude and sign of anomalies indicate region-specific changes in solar power potential in the 2040s. Our study also identifies potential region-specific impacts on hydropower production. For instance, greatly reduced precipitation over the Amazon region in the 2040s may pose an increasing challenge to keep current hydropower production while finding alternative reliable energy sources. Projected increase in precipitation over African and South Asia may grant potential opportunities in hydropower production but more precipitation may accompany with higher variability, that is, extreme rainfall events, further challenges to be prepared for extreme weather events (Uria Martinez et al., 2021) (Figures 3 and 4). This is particularly critical to some countries, such as Bhutan and Nepal, where hydropower accounts for over 90% of total electricity generation.

It is obvious that the magnitude and direction of climate change are geographically varying, and its impacts are regionally disproportionate. Our results present that many of the changes are expected to exacerbate existing and future climate impacts. For instance, less precipitation is projected over currently arid and semi-arid regions (Figure 4). Rapid warming in the north will continue its upward trend in the future (Figure 3). Increasing heat stress is projected over regions already experiencing higher heat stress (Figure 9 and Figure S12 in Supporting Information S1). Furthermore, we find that important compounding climate impacts are expected to increase across global lands. For example, the Amazon will experience severe drought, higher fire risk, and more dangerous heat stress as the Earth gets warmer. A significant increase of precipitation under warming over South Asia and Eastern Africa will lead to extreme rainfall events, while higher heat stress will be a serious public health threat. There is mounting evidence that poorer countries or people have suffered disproportionately from such individual and/or

compounding climate impacts (e.g., drought, heat stress, flood, etc.), because they either don't have the resources to mitigate or adapt to climate change, or they live in warmer climates where further warming would have a detrimental impact on their productivity and health (Diffenbaugh & Burke, 2019; King & Harrington, 2018). Our results confirm that lower income regions (or countries) will be disproportionately impacted by future climate change. The United Nations' Sustainable Development Goals (UN SDGs) include goals to reduce inequality both within and between nations (Goal 10) and to strengthen action to combat the impacts of climate change (Goal 13) (United Nations, 2015). We anticipate that our analysis of NEX-GDDP-CMIP6 further supports scientific activities associated with UN SDGs by identifying where, and to what extent, lives and livelihoods will be at risk in the future.

This study provides a comprehensive analysis of the latest NEX-GDDP-CMIP6 datasets and presents a finer scale view of future climate change and its impacts on global land at 2°C warming. The NEX-GDDP data which provides 16–64 times finer spatial information compared to native CMIP6 projections (typically $1° \sim 2°$ spatial resolution) can serve the needs of decision makers who require local climate information for various impact assessments. Our supplementary analysis clearly shows the additional spatial variations the NEX-GDDP data provide on top of the original CMIP6 GCMs (Figures S10 and S11 in Supporting Information S1). Particularly, the downscaled information is critical over the regions where spatially significant variations exist. For instance, a significant increase in precipitation over central Africa is obvious while the northern and southern African regions are projected to be stable or slightly decreasing (Figure 4b). Spatial variability of the changes is high especially over the boundaries of the contrasting precipitation changes (Figure S10b in Supporting Information S1). The spatial variation is also climate variable (or impact indicator) specific (Figure S11 in Supporting Information S1). For instance, the projected changes in temperature in the 2040s have lower spatial variability while precipitation has about 10 times higher spatial variation in the projected changes. These highlight the importance of finer spatial resolution in the climate projections. As demonstrated in heat stress and fire danger assessment, we also showcase how high temporal climate projection is critical for assessing future climate impacts. There are three important reasons why daily climate information is important in climate impact assessment. First, most climate conditions that cause serious impacts typically occur on a daily time scale rather than the average monthly condition (e.g., flash floods and heat waves). Second, many climate-related effects are cumulative and cannot be reliably assessed from monthly data since they are a result of what happens on a daily time scale—for example, the fire weather index shown in this study needs to be cumulatively computed at daily time scale (Van Wagner & Forest, 1987). Third, most agricultural, hydrologic, and other climate impact models require daily climate data to produce results relevant to real-world decision-making. In these regards, by offering a collection of global, high-resolution, bias-corrected, and seamless daily climate projections, NEX-GDDP-CMIP6 can aid in more precisely representing regional climate patterns on both the average and variation in climate as well as more thoroughly assessing future climate impacts.

4. Concluding Remarks

Understanding future climate change and its spatial heterogeneity is critical to identifying where, and to what extent, lives and livelihoods will be at risk in the future. This is a prerequisite for policy makers to prepare more actionable adaptation and mitigation plans for future climate change. This study uses the recently released NEX-GDDP-CMIP6 data set to examine the spatial heterogeneity of six projected climate variables and two climate impact variables at the point that 2°C of global warming occurs compared to pre-industrial levels. Our results reveal geographically varying patterns in the magnitude and direction of climate change. We also show that many of the changes are expected to exacerbate existing and future climate impacts. These geographically specific patterns are of policy relevance as some of the regions will experience significant climate impacts even if the 2°C goal is achieved. It naturally urges further work on identifying key hotspots, potential individual and/or compounding impacts, and advancing region-specific actionable adaptation and mitigation plans. This NEX-GDDP-based global scale analysis can be replicated at a local and regional scale, and hopefully inspires other researchers to conduct deeper investigations in their region of interest.

23284277, 2023, 5, Downloaded from https://agupubs.onlinelibrary.wiley.com/doi/10.1029/2022EF003330 by NASA Shared Services Center (NSSC), Wiley Online Library on [08/03/2024]. See the Terms and Conditions (https://onlinelibrary.wiley.com/terms-and-conditions) on Wiley Online Library for rules of use; OA articles are governed by the applicable Creative Commons License

Data Availability Statement

The NEX-GDDP data sets can be downloaded from the following links: CMIP6: https://www.nccs.nasa.gov/services/data-collections/land-based-products/nex-gddp-cmip6. CMIP5: https://www.nccs.nasa.gov/services/data-collections/land-based-products/nex-gddp. The HadCRUT (version 5.0.1.0) data set can be downloaded from the following link: https://www.metoffice.gov.uk/hadobs/hadcrut5/data/current/download.html.

Acknowledgments
Climate scenarios used were from the NEX-GDDP-CMIP6 data set, prepared by the Climate Analytics Group and NASA Ames Research Center using the NASA Earth Exchange and distributed by the NASA Center for Climate Simulation (NCCS) at Goddard Space Flight Center. T.P., H.H., W.W., B.T., A.M., I.G.B., and R.R.N. are supported by the National Aeronautics and Space Administration (NASA) under Grants to NASA Earth Exchange (NEX).

References

Abatzoglou, J. T., & Williams, A. P. (2016). Impact of anthropogenic climate change on wildfire across Western US forests. *Proceedings of the National Academy of Sciences*, *113*(42), 11770–11775. https://doi.org/10.1073/pnas.1607171113

Abatzoglou, J. T., Williams, A. P., & Barbero, R. (2019). Global emergence of anthropogenic climate change in fire weather indices. *Geophysical Research Letters*, *46*(1), 326–336. https://doi.org/10.1029/2018gl080959

Almazroui, M., Saeed, F., Saeed, S., Ismail, M., Ehsan, M. A., Islam, M. N., et al. (2021). Projected changes in climate extremes using CMIP6 simulations over SREX regions. *Earth Systems and Environment*, *5*(3), 481–497. https://doi.org/10.1007/s41748-021-00250-5

Alves de Oliveira, B. F., Bottino, M. J., Nobre, P., & Nobre, C. A. (2021). Deforestation and climate change are projected to increase heat stress risk in the Brazilian Amazon. *Communications Earth & Environment*, *2*, 1–8. https://doi.org/10.1038/s43247-021-00275-8

Asayama, M. (2009). Guideline for the prevention of heat disorder in Japan. *Global Environmental Research*, *13*(1), 19–25.

Barnett, T. P., Pierce, D. W., AchutaRao, K. M., Gleckler, P. J., Santer, B. D., Gregory, J. M., & Washington, W. M. (2005). Penetration of human-induced warming into the world's oceans. *Science*, *309*(5732), 284–287. https://doi.org/10.1126/science.1112418

Chen, D., Deng, K., Azorin-Molina, C., Yang, S., Zhang, G., & Minola, L. (2021). Terrestrial stilling will continue during the 21st century.

Deng, K., Azorin-Molina, C., Minola, L., Zhang, G., & Chen, D. (2021). Global near-surface wind speed changes over the last decades revealed by reanalyses and CMIP6 model simulations. *Journal of Climate*, *34*(6), 2219–2234. https://doi.org/10.1175/jcli-d-20-0310.1

Denson, E., Wasko, C., & Peel, M. C. (2021). Decreases in relative humidity across Australia. *Environmental Research Letters*, *16*(7), 074023. https://doi.org/10.1088/1748-9326/ac0aca

Diffenbaugh, N. S., & Burke, M. (2019). Global warming has increased global economic inequality. *Proceedings of the National Academy of Sciences*, *116*(20), 9808–9813. https://doi.org/10.1073/pnas.1816020116

Di Giuseppe, F., Pappenberger, F., Wetterhall, F., Krzeminski, B., Camia, A., Libertá, G., & San Miguel, J. (2016). The potential predictability of fire danger provided by numerical weather prediction. *Journal of Applied Meteorology and Climatology*, *55*(11), 2469–2491. https://doi.org/10.1175/jamc-d-15-0297.1

Dunne, J. P., Stouffer, R. J., & John, J. G. (2013). Reductions in labour capacity from heat stress under climate warming. *Nature Climate Change*, *3*(6), 563–566. https://doi.org/10.1038/nclimate1827

Dutta, R., Chanda, K., & Maity, R. (2022). Future of solar energy potential in a changing climate across the world: A CMIP6 multi-model ensemble analysis. *Renewable Energy*, *188*, 819–829. https://doi.org/10.1016/j.renene.2022.02.023

Fargeon, H., Pimont, F., Martin-StPaul, N., De Caceres, M., Ruffault, J., Barbero, R., & Dupuy, J. L. (2020). Projections of fire danger under climate change over France: Where do the greatest uncertainties lie? *Climatic Change*, *160*(3), 479–493. https://doi.org/10.1007/s10584-019-02629-w

Fauchald, P., Park, T., Tømmervik, H., Myneni, R., & Hausner, V. H. (2017). Arctic greening from warming promotes declines in caribou populations. *Science Advances*, *3*(4), e1601365. https://doi.org/10.1126/sciadv.1601365

Giorgi, F., & Francisco, R. (2000). Evaluating uncertainties in the prediction of regional climate change. *Geophysical Research Letters*, *27*(9), 1295–1298. https://doi.org/10.1029/1999gl011016

Greve, P., Orlowsky, B., Mueller, B., Sheffield, J., Reichstein, M., & Seneviratne, S. I. (2014). Global assessment of trends in wetting and drying over land. *Nature Geoscience*, *7*(10), 716–721. https://doi.org/10.1038/ngeo2247

Hahn, L. C., Armour, K. C., Zelinka, M. D., Bitz, C. M., & Donohoe, A. (2021). Contributions to polar amplification in CMIP5 and CMIP6 models. *Frontiers of Earth Science*, *725*. https://doi.org/10.3389/feart.2021.710036

Hempel, S., Frieler, K., Warszawski, L., Schewe, J., & Piontek, F. (2013). A trend-preserving bias correction–the ISI-MIP approach. *Earth System Dynamics*, *4*(2), 219–236. https://doi.org/10.5194/esd-4-219-2013

Hsu, A., Sheriff, G., Chakraborty, T., & Manya, D. (2021). Disproportionate exposure to urban heat Island intensity across major US cities. *Nature Communications*, *12*, 1–11. https://doi.org/10.1038/s41467-021-22799-5

Jain, P., Castellanos-Acuna, D., Coogan, S. C., Abatzoglou, J. T., & Flannigan, M. D. (2022). Observed increases in extreme fire weather driven by atmospheric humidity and temperature. *Nature Climate Change*, *12*(1), 63–70. https://doi.org/10.1038/s41558-021-01224-1

King, A. D., & Harrington, L. J. (2018). The inequality of climate change from 1.5 to 2°C of global warming. *Geophysical Research Letters*, *45*(10), 5030–5033. https://doi.org/10.1029/2018gl078430

Kirchner, I., Stenchikov, G. L., Graf, H.-F., Robock, A., & Antuña, J. C. (1999). Climate model simulation of winter warming and summer cooling following the 1991 Mount Pinatubo volcanic eruption. *Journal of Geophysical Research*, *104*(D16), 19039–19055. https://doi.org/10.1029/1999jd900213

Lemke, B., & Kjellstrom, T. (2012). Calculating workplace WBGT from meteorological data: A tool for climate change assessment. *Industrial Health*, *50*(4), 267–278. https://doi.org/10.2486/indhealth.ms1352

Li, C., Zwiers, F., Zhang, X., Li, G., Sun, Y., & Wehner, M. (2021). Changes in annual extremes of daily temperature and precipitation in CMIP6 models. *Journal of Climate*, *34*(9), 3441–3460. https://doi.org/10.1175/jcli-d-19-1013.1

Li, H., Li, Z., Chen, Y., Xiang, Y., Liu, Y., Kayumba, P. M., & Li, X. (2021). Drylands face potential threat of robust drought in the CMIP6 SSPs scenarios. *Environmental Research Letters*, *16*(11), 114004. https://doi.org/10.1088/1748-9326/ac2bce

Lu, J., Vecchi, G. A., & Reichler, T. (2007). Expansion of the Hadley cell under global warming. *Geophysical Research Letters*, *34*(6), L06805. https://doi.org/10.1029/2006gl028443

Madsen, H., Lawrence, D., Lang, M., Martinkova, M., & Kjeldsen, T. R. (2014). Review of trend analysis and climate change projections of extreme precipitation and floods in Europe. *Journal of Hydrology*, *519*, 3634–3650. https://doi.org/10.1016/j.jhydrol.2014.11.003

Martinez, A., & Iglesias, G. (2022). Climate change impacts on wind energy resources in North America based on the CMIP6 projections. *Science of the Total Environment*, *806*, 150580. https://doi.org/10.1016/j.scitotenv.2021.150580

Masson-Delmotte, V., Zhai, P., Pirani, A., Connors, S. L., Péan, C., Berger, S., et al. (2021). *Climate change 2021: The physical science basis. Contribution of working group I to the sixth assessment report of the intergovernmental panel on climate change*. IPCC.

23284277, 2023, 5, Downloaded from https://agupubs.onlinelibrary.wiley.com/doi/10.1029/2022EF003330 by NASA Shared Services Center (NSSC), Wiley Online Library on [08/03/2024]. See the Terms and Conditions (https://onlinelibrary.wiley.com/terms-and-conditions) on Wiley Online Library for rules of use; OA articles are governed by the applicable Creative Commons License

Masson-Delmotte, V., Zhai, P., Pörtner, H.-O., Roberts, D., Skea, J., Shukla, P. R., et al. (2018). Global warming of 1.5°C. An IPCC special report on the impacts of global warming of 1.

McCrystall, M. R., Stroeve, J., Serreze, M., Forbes, B. C., & Screen, J. A. (2021). New climate models reveal faster and larger increases in Arctic precipitation than previously projected. *Nature Communications*, *12*, 1–12. https://doi.org/10.1038/s41467-021-27031-y

McVicar, T. R., Roderick, M. L., Donohue, R. J., Li, L. T., Van Niel, T. G., Thomas, A., et al. (2012). Global review and synthesis of trends in observed terrestrial near-surface wind speeds: Implications for evaporation. *Journal of Hydrology*, *416*, 182–205. https://doi.org/10.1016/j.jhydrol.2011.10.024

Morice, C. P., Kennedy, J. J., Rayner, N. A., Winn, J. P., Hogan, E., Killick, R. E., et al. (2021). An updated assessment of near-surface temperature change from 1850: The HadCRUT5 data set. *Journal of Geophysical Research: Atmospheres*, *126*(3), e2019JD032361. https://doi.org/10.1029/2019jd032361

Navarro-Racines, C., Tarapues, J., Thornton, P., Jarvis, A., & Ramirez-Villegas, J. (2020). High-resolution and bias-corrected CMIP5 projections for climate change impact assessments. *Scientific Data*, *7*, 1–14. https://doi.org/10.1038/s41597-019-0343-8

O'Neill, B. C., Tebaldi, C., van Vuuren, D. P., Eyring, V., Friedlingstein, P., Hurtt, G., et al. (2016). The scenario model intercomparison project (ScenarioMIP) for CMIP6. *Geoscientific Model Development*, *9*, 3461–3482. https://doi.org/10.5194/gmd-9-3461-2016

Panthou, G., Lebel, T., Vischel, T., Quantin, G., Sane, Y., Ba, A., et al. (2018). Rainfall intensification in tropical semi-arid regions: The Sahelian case. *Environmental Research Letters*, *13*(6), 064013. https://doi.org/10.1088/1748-9326/aac334

Park, J. Y., Bader, J., & Matei, D. (2015). Northern-hemispheric differential warming is the key to understanding the discrepancies in the projected Sahel rainfall. *Nature Communications*, *6*(1), 1–8. https://doi.org/10.1038/ncomms6985

Park, T., Chen, C., Macias-Fauria, M., Tømmervik, H., Choi, S., Winkler, A., et al. (2019). Changes in timing of seasonal peak photosynthetic activity in northern ecosystems. *Global Change Biology*, *25*(7), 2382–2395. https://doi.org/10.1111/gcb.14638

Parsons, L. A. (2020). Implications of CMIP6 projected drying trends for 21st century Amazonian drought risk. *Earth's Future*, *8*(10), e2020EF001608. https://doi.org/10.1029/2020ef001608

Pierce, D. W., Cayan, D. R., & Thrasher, B. L. (2014). Statistical downscaling using localized constructed analogs (LOCA). *Journal of Hydrometeorology*, *15*(6), 2558–2585. https://doi.org/10.1175/jhm-d-14-0082.1

Raymond, C., Matthews, T., & Horton, R. M. (2020). The emergence of heat and humidity too severe for human tolerance. *Science Advances*, *6*(19), eaaw1838. https://doi.org/10.1126/sciadv.aaw1838

Richardson, T. B., Forster, P. M., Andrews, T., Boucher, O., Faluvegi, G., Fläschner, D., et al. (2018). Carbon dioxide physiological forcing dominates projected eastern Amazonian drying. *Geophysical Research Letters*, *45*(6), 2815–2825. https://doi.org/10.1002/2017gl076520

Riley, K. L., Williams, A. P., Urbanski, S. P., Calkin, D. E., Short, K. C., & O'Connor, C. D. (2019). Will landscape fire increase in the future? A systems approach to climate, fire, fuel, and human drivers. *Current Pollution Reports*, *5*(2), 9–24. https://doi.org/10.1007/s40726-019-0103-6

Schleussner, C.-F., Lissner, T. K., Fischer, E. M., Wohland, J., Perrette, M., Golly, A., et al. (2016). Differential climate impacts for policy-relevant limits to global warming: The case of 1.5°C and 2°C. *Earth system dynamics*, *7*, 327–351. https://doi.org/10.5194/esd-7-327-2016

Serreze, M. C., & Barry, R. G. (2011). Processes and impacts of Arctic amplification: A research synthesis. *Global and Planetary Change*, *77*(1–2), 85–96. https://doi.org/10.1016/j.gloplacha.2011.03.004

Solomon, S., Manning, M., Marquis, M., & Qin, D. (2007). *Climate change 2007-the physical science basis: Working group I contribution to the fourth assessment report of the IPCC*. Cambridge university press.

Stocker, T. F., Qin, D., Plattner, G.-K., Tignor, M., Allen, S. K., Boschung, J., et al. (2013). *IPCC, 2013: Climate change 2013: The physical science basis. Contribution of working group I to the fifth assessment report of the intergovernmental panel on climate change*. Cambridge University Press.

Sutton, R. T., Dong, B., & Gregory, J. M. (2007). Land/sea warming ratio in response to climate change: IPCC AR4 model results and comparison with observations. *Geophysical Research Letters*, *34*(2), L02701. https://doi.org/10.1029/2006gl028164

Taylor, K. E., Stouffer, R. J., & Meehl, G. A. (2012). An overview of CMIP5 and the experiment design. *Bulletin of the American Meteorological Society*, *93*(4), 485–498. https://doi.org/10.1175/bams-d-11-00094.1

Thrasher, B., Maurer, E. P., McKellar, C., & Duffy, P. B. (2012). Bias correcting climate model simulated daily temperature extremes with quantile mapping. *Hydrology and Earth System Sciences*, *16*(9), 3309–3314. https://doi.org/10.5194/hess-16-3309-2012

Thrasher, B., Wang, W., Michaelis, A., Melton, F., Lee, T., & Nemani, R. (2022). NASA global daily downscaled projections, CMIP6. *Scientific Data*, *9*, 1–6. https://doi.org/10.1038/s41597-022-01393-4

UNFCCC. (2015). Adoption of the Paris agreement. *25th session Paris*, *30*.

United Nations. (2015). *Transforming our world: The 2030 agenda for sustainable development*. United Nations.

Uria Martinez, R., Johnson, M., & Shan, R. (2021). *US hydropower market report (January 2021 edition)*. Oak Ridge National Laboratory (ORNL).

Vandal, T., Kodra, E., Ganguly, S., Michaelis, A., Nemani, R., & Ganguly, A. R. (2017). DeepSD: Generating high resolution climate change projections through single image super-resolution. In *Proceedings of the 23rd ACM SIGKDD International Conference on Knowledge Discovery and Data Mining* (pp. 1663–1672).

Van Wagner, C. E., & Forest, P. (1987). Development and structure of the canadian forest fire weather index system. In C F. Serv (Ed.), *Forestry technical report*. Citeseer.

Vautard, R., Cattiaux, J., Yiou, P., Thépaut, J.-N., & Ciais, P. (2010). Northern hemisphere atmospheric stilling partly attributed to an increase in surface roughness. *Nature Geoscience*, *3*(11), 756–761. https://doi.org/10.1038/ngeo979

Vautard, R., Gobiet, A., Sobolowski, S., Kjellström, E., Stegehuis, A., Watkiss, P., et al. (2014). The European climate under a 2°C global warming. *Environmental Research Letters*, *9*(3), 034006. https://doi.org/10.1088/1748-9326/9/3/034006

Westervelt, D. M., Horowitz, L. W., Naik, V., Golaz, J.-C., & Mauzerall, D. L. (2015). Radiative forcing and climate response to projected 21st century aerosol decreases. *Atmospheric Chemistry and Physics*, *15*(22), 12681–12703. https://doi.org/10.5194/acp-15-12681-2015

Zeng, Z., Ziegler, A. D., Searchinger, T., Yang, L., Chen, A., Ju, K., et al. (2019). A reversal in global terrestrial stilling and its implications for wind energy production. *Nature Climate Change*, *9*(12), 979–985. https://doi.org/10.1038/s41558-019-0622-6

References From the Supporting Information

World Meteorological Organization (WMO). (2018). *Guide to climatological practices*. World Meteorological Organization.

Zelinka, M. D., Myers, T. A., McCoy, D. T., Po-Chedley, S., Caldwell, P. M., Ceppi, P., et al. (2020). Causes of higher climate sensitivity in CMIP6 models. *Geophysical Research Letters*, *47*(1), e2019GL085782. https://doi.org/10.1029/2019gl085782

23284277, 2023, 5, Downloaded from https://agupubs.onlinelibrary.wiley.com/doi/10.1029/2022EF003330 by NASA Shared Services Center (NSSC), Wiley Online Library on [08/03/2024]. See the Terms and Conditions (https://onlinelibrary.wiley.com/terms-and-conditions) on Wiley Online Library for rules of use; OA articles are governed by the applicable Creative Commons License